Inorganic Chemistry

Article

Role of the Hydroxyl−Water Hydrogen-Bond Network in Structural Transitions and Selectivity toward Cesium in $Cs_{0.38}(D_{1.08}H_{0.54})SiTi_2O_7 \cdot (D_{0.86}H_{0.14})_2O$ Crystalline Silicotitanate

Aaron J. Celestian,*,† John B. Parise,† Ronald I. Smith,‡ Brian H. Toby,§ and Abraham Clearfield⊥

Department of Geosciences, Center for Environmental and Molecular Sciences, Stony Brook University, Stony Brook, New York 11794-2100, ISIS Neutron Facility, Rutherford Appleton Laboratory, Chilton, Didcot, Oxon OX11 0QX, U.K., Advanced Photon Source, Argonne National Laboratory, Argonne Illinois 60439-4856, and Department of Chemistry, Texas A&M University, College Station, Texas 77843-3133

The crystal structure of the selective Cs^+ ion exchanger $D_{1.6}H_{0.4}Ti_2SiO_7 \cdot D_{2.66}H_{0.34}O_{1.5}$, known as crystalline silicotitanate or CST, has been determined in both native (D−CST) and in the Cs^+-exchanged forms ((Cs, D)−CST) from angle-dispersive and time-of-flight neutron diffraction studies. The final fully exchange Cs^+ form transformed from D−CST with unit cell parameters $a = 11.0704(3)$ Å $c = 11.8917(5)$ Å and space group $P4_2/mbc$, to one with $a = 7.8902$-(1) Å $c = 11.9051(4)$ Å and space group $P4_2/mcm$. Rietveld structure refinements of both D−CST and (Cs, D)−CST suggest the transition, and ultimately the selectivity, is driven by changes in the positions of water molecules, in response to the initial introduction of Cs^+. The changes in water position appear to disrupt the D−O−O−D dihedral associated with the CST framework in space group $P4_2/mbc$ which ultimately leads to the structural transition. The new geometric arrangement of the water−deuteroxyl network in (Cs, D)−CST suggests that D_{water}−$D_{deuteroxyl}$ repulsion forced by Cs^+ exchange drives the structural transformation.

Introduction

Crystalline silicotitanates (CST) with the mineral sitinakite topology[1,2] along with the H-exchanged (H−CST) and Nb-substituted forms,[2−5] are being tested as possible ion exchangers for the sequestration of ^{137}Cs and ^{90}Sr from radioactive nuclear waste solutions.[6−16] The selectivity for Cs^+, even in highly alkaline solutions of 1−7 M NaOH and

NaNO$_3$,[10] and its resistance to crystalline deterioration by both high radiation fields and high pH (>12) solutions, make H−CST a promising candidate for selective removal of Cs^+ from waste solutions. The targeted removal of Cs^+ from solutions would reduce the overall solution activity and make for safer long-term storage.

Ion sequestration processes in crystalline molecular sieves are inherently time and pathway dependent because the

* To whom correspondence should be addressed. E-mail: aaron.celestian@gmail.com.
† Stony Brook University.
‡ Rutherford Appleton Laboratory.
§ Argonne National Laboratory.
⊥ Texas A&M University.
 (1) Menshikov, Y. P.; Sokolova, E. V.; Yegorov-Tismenko, Y. K.; Khomyakov, A. P.; Polezhaeva, L. I. *Zap. Vses. Mineral. Obshch.* **1992**, *121*, 94−99.
 (2) Poojary, D. M.; Cahill, R. A.; Clearfield, A. *Chem. Mater.* **1994**, *6*, 2364−2368.
 (3) Bortun, A. I.; Bortun, L. N.; Khainakov, S. A.; Clearfield, A.; Trobajo, C.; Garcia, J. R. *Solvent Extr. Ion. Exc.* **1999**, *17*, 649−675.
 (4) Clearfield, A.; Tripathi, A.; Nyman, M.; Medvedev, D. *Abstr. Pap. Am. Chem. S.* **2002**, *224*, U696−U696.
 (5) Tripathi, A.; Medvedev, D. G.; Nyman, M.; Clearfield, A. *J. Solid State Chem.* **2003**, *175*, 72−83.
 (6) Clearfield, A.; Sylvester, P.; Bluhm, E.; Bortun, A.; Bortun, L. *Abstr. Pap. Am. Chem. S.* **1999**, *218*, U1061−U1061.

 (7) Hritzko, B. J.; Walker, D. D.; Wang, N. H. L. *AICHE J.* **2000**, *46*, 552−564.
 (8) Marinin, D. V.; Brown, G. N. *Waste Manage.* **2000**, *20*, 545−553.
 (9) Zheng, Z.; Anthony, R. G.; Miller, J. E. *Ind. Eng. Chem. Res.* **1997**, *36*, 2427−2434.
 (10) Zheng, Z. X.; Gu, D.; Anthony, R. G.; Klavetter, E. *Ind. Eng. Chem. Res.* **1995**, *34*, 2142−2147.
 (11) Anthony, R. G.; Dosch, R. G.; Gu, D.; Philip, C. V. *Ind. Eng. Chem. Res.* **1994**, *33*, 2702−2705.
 (12) McCabe, D. J. *Abstr. Pap. Am. Chem. S.* **1997**, *214*, 100-NUCL.
 (13) Wilmarth, W. R.; Mills, J. T.; Dukes, V. H.; Fondeur, F. F.; Walker, D. D. *Abstr. Pap. Am. Chem. S.* **2001**, *221*, U482−U482.
 (14) Wilmarth, W. R.; Hang, T.; Walker, D. D.; Mills, J. T.; Dukes, V. H.; Fink, S. D. *Abstr. Pap. Am. Chem. S.* **2000**, *219*, U761−U761.
 (15) Sylvester, P.; Clearfield, A. In *American Chemical Society Symposium*; Ellen, P. G., WHeineman, W. R., Eds.; American Chemical Society: Washington, DC, 2000; Vol. 778, pp 133−145.
 (16) Clearfield, *Solid State Sci.* **2001**, *3*, 103−112.

structures of these materials often distort to accommodate the exchanged ions (e.g., gismondine[17−21]). The irreversibility of Cs^+ exchange in CST is a consequence of the site-selective exchange pathway that ultimately results in high affinity for Cs^+.[22] The mechanisms and dynamics that control ion diffusion processes in zeolitic molecular sieves have only been studied recently with in situ diffraction techniques.[22−25] These time-resolved X-ray diffraction (XRD) studies demonstrated that the structural transformation which occur during ion exchange serve to enhance the exchange capacity and/or ion selectivity of the material. Diffraction techniques, either X-ray or neutron, are well suited for studies involving structural and chemical changes because both techniques probe the scattering efficiencies of atoms, which are interpreted as atom type, and their positions within a unit cell.

The work presented here includes well-characterized end member structures, as these are an essential prerequisite for successful Rietveld structure refinements of the time-resolved data because the latter necessarily views a more limited region of reciprocal space. Also, the precision of crystallographic information obtained from structural analysis of time-resolved data is further compromised by reduced counting statistics, decreased peak-to-background ratios, multiple phase components, and scattering from ion-exchange media and the in situ cell. Such time-resolved studies elucidate the mechanistic and dynamic nature of cation diffusion processes in zeolites and zeolitic molecular sieves.

The CST material is synthesized in the Na form (Na−CST, $Na_2Ti_2SiO_7 \cdot 2H_2O$),[2] and then H^+ exchanged (H−CST) in preparation for Cs^+ absorption.[26] In the general CST form,[27] the structure consists of columns of Ti oxide octahedra centered on a 4-fold axis parallel to [001] (Figure 1). The Ti−O octahedra columns are composed of a cluster of Ti_4O_{16} groups collectively generating Ti_4O_4 cubane-like subunits. These cubane-like groups in the H−CST structure deviate from cube geometry (Figure 2). Columns are connected by silica tetrahedra to form one eight-member ring (8MR) channel along [001] (Figure 1) and three perpendicular 6MR channels along [100], [010], and [110] The 6MR channels have a long axis/short axis (L/S) ratio of 1.25, defined from $L = O4−O4 = 6.02$ Å and $S = O1−O3 = 4.87$ Å, and have only been observed to be large enough to

(17) Nery, J. G.; Mascarenhas, Y. P.; Cheetham, A. K. *Micropor. Mesopor. Mater.* **2003**, *57*, 229−248.
(18) Bauer, T.; Baur, W. H. *Euro. J. Min.* **1998**, *10*, 133−147.
(19) Celestian, A. J.; Parise, J. B.; Goodell, C.; Tripathi, A.; Hanson, J. *Chem. Mater.* **2004**, *16*, 2244−2254.
(20) Celestian, A. J.; Parise, J. B.; Tripathi, A.; Kvick, A.; Vaughan, G. M. B. *Acta Crystallogr. C* **2003**, *59*, I74−I76.
(21) Tripathi, A.; Parise, J. B.; Kim, S. J.; Lee, Y.; Johnson, G. M.; Uh, Y. S. *Chem. Mater.* **2000**, *12*, 3760−3769.
(22) Celestian, A. J.; Medvedev, D. G.; Tripathi, A.; Parise, J. B.; Clearfield, A. *Nucl. Instrum. Methods B* **2005**, *238*, 61−69.
(23) Celestian, A. J. Masters Thesis, Stony Brook University, 2002.
(24) Parise, J. B.; Cahill, C.; Chen, J. *Abstr. Pap. Am. Chem. S.* **1998**, *215*, U811−U811.
(25) Lee, Y.; Reisner, B. A.; Hanson, J. C.; Jones, G. A.; Parise, J. B.; Corbin, D. R.; Toby, B. H.; Freitag, A.; Larese, J. Z. *J. Phys. Chem. B* **2001**, *105*, 7188−7199.
(26) Bortun, A. I.; Bortun, L. N.; Clearfield, A. *Solvent Extr. Ion Exc.* **1996**, *14*, 341−354.
(27) Pertierra, P.; Salvado, M. A.; Garcia-Granda, S.; Bortun, A. I.; Clearfield, A. *Inorg. Chem.* **1999**, *38*, 2563−2566.
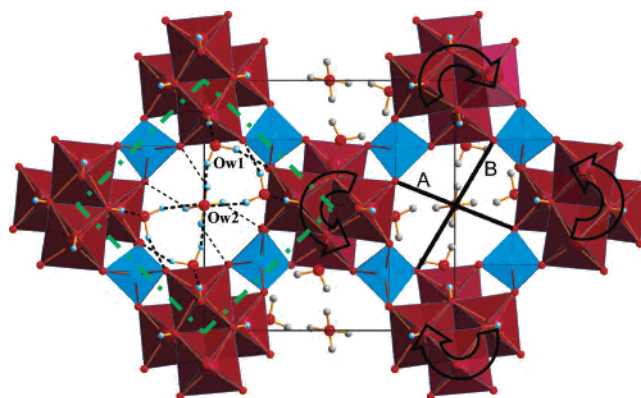
Figure 1. Crystal structure of D−CST refined from current study. View is down the 8MR. [001] Black box is the unit cell of D−CST, the green dash-dot box is the overlay of the (Cs, D)−CST unit cell. Heavy dashed lines in the left 8MR channel are deuteron bonds from deuteroxyl and water (Ow1), and light dashed lines are deuteron bonds from Ow2 to framework O^{2-}. Block arrows indicate how the Ti−O octahedra columns rotate to obtain the (Cs, D)−CST structure. Water deuterons of site Ow1 point toward the center of the 8MR. Lines B and A are the measured L/S ratio (1.53). Ti (maroon), Si (blue), O (red), D|H (gray).
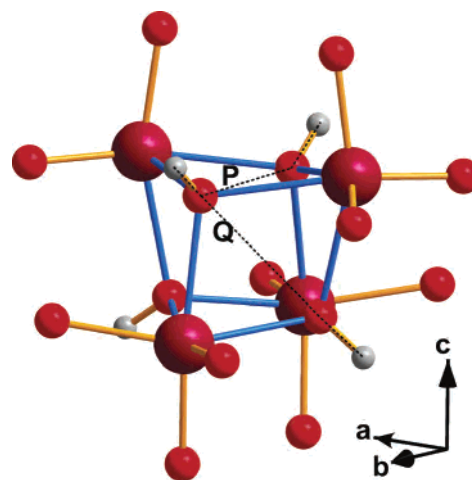

Figure 2. Cubane-like unit of D−CST. Dihedral angle for D−O−O−D along line P have an angle of 4.089(2)° and along Q are 0.605(1)°. Distorted square planes of Ti−O measured from internal Ti−O−Ti angles of faces perpendicular to [110], [1−10], and [001] are 103.35(1)°, 105.26(1)°, and 106.81(1)°, respectively.

accommodate nothing larger Na^+ cations. The diameters of the elliptical 8MR channels are 6.9 Å for the long-axis ($L = O1−O1$) and 4.5 Å along the short axis ($S = O3−O3$) (L/S = 1.53; Lines A and B, Figure 1). In H−CST, the 8MR channels are solely filled with interstitial water molecules that form a H-bond network anchored at the framework hydroxyls. The charge balancing H^+ sites form hydroxides positioned at the edge share union vertex of three Ti octahedra (Figure 2). The vertex sites are the O^{2-} corners of the cubane-like unit. It is these H^+ sites are readily exchangeable with larger cations in the 8MR channel.

The previous time-resolved XRD investigations of Cs^+ exchange into H−CST illustrated that the exchange process is selective by crystallographic site and accompanied by structural transformations.[22] There are two crystallographically distinct Cs^+ sites in (Cs, H)−CST: one in the center of the 8MR (Cs1) with 8-fold coordination to framework O^{2-}, and one outside of the 8MR (Cs2) with 4-fold

coordination to framework O^{2-} and 2-fold coordination with interstitial water.[2] The Cs1 site in the H−CST phase cannot accommodate the large Cs^+ ionic radius without structural distortion because of unacceptable short Cs−O bond lengths of less than 3 Å; these short distances result in unexpectedly large bond valence sums, with valences greater than three. In contrast, site Cs2 is able to obtain acceptable bonding geometry but is less energetically favorable for occupancy because of its lower coordination environment. The time-resolved XRD work illustrated that Cs^+ first exchanged into site Cs2 with a concomitant change in the crystal structure to form circular (L/S = 1) 8MR.[22] After site Cs2 filled to ~15% occupancy, site Cs1 became favored for ion exchange due to the structural transformation, which allowed Cs1−O bond distances of ~3.18 Å. The reverse exchange, H^+ into Cs−CST, was also attempted in situ using 5 M HCl, but no Cs^+ removal was measured. The structural transformation that favors Cs^+ at Cs1 likely explains the difficulty of back exchanged by H^+. The exchange mechanisms could not be fully understood previously because the positions and orientations of the H^+ sites on the water and hydroxyls could not be resolved by X-ray diffraction techniques. In order to understand the dynamics and mechanics of the Cs^+ exchange process in CST and the origin of the structural transformations, the H^+ positions of the hydroxyl sites and water orientations of Cs−CST must be determined.

Experimental Methods

Sample Preparation. The starting material Na−CST (a = 7.8082(2) Å c = 11.9735(4) Å, $P4_2/mcm$) was first characterized by Poojary et al. (1994)[2] and was synthesized according to the procedures of Medvedev et al. (2004).[28] Starting gels of molar oxide composition 1.0 TiO_2:1.98 SiO_2:6.77 Na_2O:218 (DI)H_2O were prepared by first adding 6.6 mL of $TiCl_4$ to 23.30 mL of H_2O in a plastic bottle (A) of 500 mL capacity. To this mixture in bottle (A), 40 mL of 30% H_2O_2 in H_2O was added followed by 150 mL of deionized H_2O and 40 mL of 10 M NaOH solution. Then in another 500 mL plastic bottle (B) containing 200 mL of 1 M NaOH, 4.3 g of colloidal silica (Ludox AS-40) was added. The pH of the total solution was adjusted by adding 1 M NaOH solution until a pH of 12.6−12.8 was achieved. The gel was not allowed to age and was immediately treated hydrothermally in 30 and 100 mL Teflon lined stainless steel Parr autoclaves at 210 °C for 10 days in a convection oven. The resulting white powder was filtered using a vacuum flask with 0.45 μm filter paper, rinsed with deionized water, and left to air-dry at room temperature. XRD data were collected on all synthesized samples and showed Na−CST to be the dominant phase. A small amount of impurity phase was present in all preparations. The strongest peak from the impurity phase in the XRD patterns was <1% of the strongest peak from Na−CST. Peaks from the impurity phase present could not be indexed on the basis of unit cells corresponding to known impurities phases such as sodium nonatitanate (SNT, $Na_4Ti_9O_{20} \cdot xH_2O$)[29] or sodium titanium oxide silicate (STOS, Na_2TiSiO_5).[30] Attempts to determine unit cell parameters using standard powder indexing software[31] were
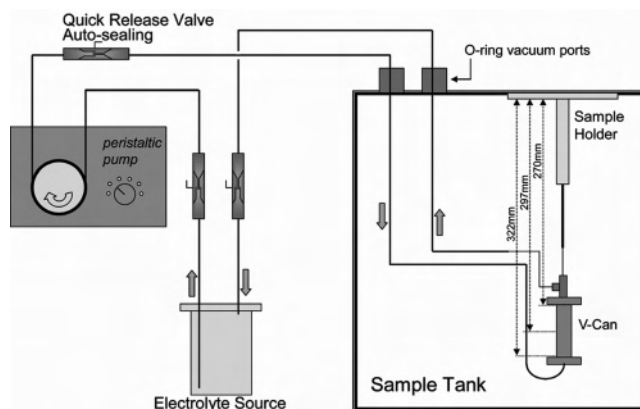

Figure 3. Neutron diffraction environmental cell. Direction of flow is indicated by arrows.

also unsuccessful. These extra peaks from the impurity phase did not change in position or intensity after ion exchange, and from this observation, it was concluded that no Cs^+ ion exchange occurred in the impurity phase and did not affect the total uptake of Cs^+ from solution.

In order to make the CST framework assessable for the exchange of Cs, Na−CST must first be proton-exchanged. For structural studies by neutron diffraction, it is preferable to use the ^{2}H (D) isotope, rather than using the ^{1}H isotope, due to its smaller incoherent scattering cross-section.[32] The incoherent scattering from the ^{1}H isotope is manifested in much higher backgrounds in the neutron diffraction pattern. To minimize exchange of D by ^{1}H in the atmosphere, all ion-exchange experiments must be performed in D_2O solutions and in controlled environmental chambers, such as a N_2 glovebox or in situ flow-through cell used in this study. Powder diffraction patterns of all samples were collected before and after exchange on a Scintag Pad-X diffractometer to ensure consistency between X-ray and neutron Cs^+ ion exchange experiments.

In Situ Ion Exchange Time-of-Flight Neutron Diffraction. The medium-resolution Polaris beamline at the ISIS spallation neutron source,[33] Rutherford Appleton Laboratory was chosen for diffraction studies because of the high flux of neutrons, rapid data acquisition times, and a beamline geometry optimized for in situ studies. The Cs^+ exchange into D−CST required the development of a flow-through cell for neutron in situ ion-exchange studies (Figure 3). The flow-through cell was assembled at Stony Brook University and was designed to minimize the amount of ion-exchange solution used and solution's exposure to the atmosphere. The cell design had to preclude the possible spillage of activated Cs solutions during the exchange experiments. Finally, an airtight design was also required, due to the location of the cell in the beam bath, which is in high vacuum to minimize neutron absorption and scatter by air. The entire flow-through system consists of a variable low-flow peristaltic pump, Teflon exchange solution container (fitted with flow and return ports), plastic tubing with quick release auto-sealing valves, 1/16 in. and 1/8 in. stainless steel pipe inside the sample tank, V can for the sample containment, and glass wool on the top and bottom of the V can to prevent sample loss. The outside top and bottom of the V sample can was covered with neutron absorbing Cd metal to prevent neutron scatter from the stainless steel threaded

(28) Medvedev, D. G.; Tripathi, A.; Clearfield, A.; Celestian, A. J.; Parise, J. B.; Hanson, J. *Chem. Mater.* **2004**, *16*, 3659−3666.
(29) Yates, S. F.; Sylvester, P. *Separ. Sci. Technol.* **2001**, *36*, 867−883.
(30) Nyman, H.; Okeeffe, M.; Bovin, J. O. *Acta Crystallogr. B* **1978**, *34*, 905−906.
(31) Shirley, R. 9.33 ed. Guildford, 2000.

(32) Bacon, G. E. *Neutron Diffraction*, 1st ed.; Oxford University Press: London, 1955.
(33) Hull, S.; Smith, R. I.; David, W. I. F.; Hannon, A. C.; Mayers, J.; Cywinski, R. *Physica B* **1992**, *180*, 1000−1002.

caps. The solution flow rate was maintained at a constant 0.44 mL/min.

Diffraction data were collected over 30 min intervals at room temperature to monitor the ion-exchange processes. First, ~2.5 g of the as-synthesized Na−CST was packed into a V can with dimensions 62.5 mm in length and 6.5 mm in diameter and placed inside the sample tank. The sample was first wetted with a D_2O solution, and then 100 mL of 1M DCl in D_2O solution was added to the exchange solution container. At the experimental rate of flow of 0.44 mL/min, it was estimated the entire contents of solution container would pass through the sample every 132 min. The exchange solution was refreshed three times every 100 min to maintain a high DCl concentration and to ensure full D^+ exchange. The Cs^+ exchange into D−CST experiment was started only after the indexed diffraction data suggested full D^+ exchange occurred which were compared to calculated D−CST time-of-flight neutron data. Next, 0.05 g of CsCl was added to 100 mL of D_2O and placed in the exchange solution container. The flow rate was not adjusted, and data collection did not stop between the exchange experiments. The solution was refreshed a total of 10 times, with ~3−5 h between refreshed solution changes to ensure full Cs^+ exchange. The final diffraction patterns for D−CST and (Cs, D)−CST were each collected for 22 and 32 h, respectively.

Ex Situ Ion-Exchange Angle-Dispersive Neutron Diffraction. For the experiment at the BT-1 beamline at the NIST Center for Neutron Research at the National Institute for Standards and Technology, ion-exchanged samples were prepared ex situ in a N_2-atmosphere glovebox. Hydrogen gas levels were monitored to less than 0.1 wt %. Na−CST was converted to the D−CST by agitating 5 g of Na−CST in 200 mL of 0.1 M DCl in D_2O solution for 30 min and was repeated three times to ensure full D^+ exchange. After D^+ exchange, the powder was filtered and rinsed with D_2O. Next, D−CST was Cs^+ exchanged using a 0.1 M CsCl in D_2O solution and agitated by hand for 30 min. After Cs^+ exchange, the powder was filtered and rinsed with D_2O. This step was repeated twice to ensure full Cs^+ exchange. Approximately 0.01 g of powder was removed and characterized by XRD to confirm full exchange prior to neutron diffraction experiments, and the remaining samples were then sealed in polypropylene containers.

Neutron powder diffraction data were collected using the BT-1 32-detector neutron powder diffractometer. A Ge(311) monochromator with a 75° takeoff angle, $\lambda = 2.0787(2)$ Å, and in-pile collimation of 15 min of arc were used. Data were collected over the range of 1.3−166.3° 2θ with a step size of 0.05°. The instrument is described in the NCNR web site (http://www.ncnr.nist.gov/). The sample was loaded in a V can sample container of length 50 mm and diameter 9.2 mm. Data were collected at ~23 °C and 1 atm. The diffraction patterns for D−CST and (Cs, D)−CST were each collected for 12 and 8 h, respectively.

Results

The structures of D−CST and (Cs, D)−CST (Tables 1−5) were refined by the Rietveld method[34] from both time-of-flight and angle-dispersive neutron diffraction data (Figures 4 and 5). The D−CST structure was determined to establish a baseline against which to compare the Cs-exchanged form and to determine the instrumental and sample contributions to profile parameters for the diffraction pattern. This carefully refined baseline structure provided some initial constraints for the structure models derived from more compromised

(34) Rietveld, H. M. *J. Appl. Crystallogr.* **1969**, *2*, 65−71.

Table 1. Refinement Statistics for Time-of-Flight and Angle-Dispersive Diffraction Data

crystal name	D−CST	(Cs, D)−CST	D−CST	(Cs, D)−CST
space group	P4$_2$/mbc	P4$_2$/mcm	P4$_2$/mbc	P4$_2$/mcm
radiation	time-of-flight	time-of-flight	$\lambda = 2.0787(2)$ Å	$\lambda = 2.0787(2)$ Å
a (Å)	11.0704(3)	7.8602(1)	11.0678(3)	7.8510(3)
b (Å)	11.0704(3)	7.8602(1)	11.0678(3)	7.8510(3)
c (Å)	11.8917(5)	11.9051(4)	11.9047(4)	11.8957(8)
α	90°	90°	90°	90°
β	90°	90°	90°	90°
γ	90°	90°	90°	90°
V (Å^3)	1457.38(8)	735.53(2)	1458.29(7)	733.23(5)
refln range	0 ≤ h ≤ 15	0 ≤ h ≤ 10	0 ≤ h ≤ 10	0 ≤ h ≤ 7
	0 ≤ k ≤ 11	0 ≤ k ≤ 7	0 ≤ k ≤ 7	0 ≤ k ≤ 5
	0 ≤ l ≤ 16	0 ≤ l ≤ 16	0 ≤ l ≤ 10	0 ≤ l ≤ 10
no. of reflns	949	440	302	174
χ^2	4.264	4.86	2.597	1.492
fitted wRp^a	0.0099	0.0059	0.0859	0.0676
fitted Rp^a	0.0112	0.0067	0.0668	0.0548
bknd wRp^a	0.0185	0.0075	0.1036	0.0709
bknd Rp^a	0.0192	0.0067	0.0806	0.0638

^{a} Values are averaged over all detector banks for time-of-flight diffraction data.

Table 2. Atomic Coordinates, Isotropic Displacement, and Fractional Occupancy Parameters for D−CST

name	x	y	z	U_{iso} (Å^2)	fractional occupancy
D1|H1	−0.022(1)	0.178(9)	0.1294(8)	0.026(6)	0.929(3)|0.070(1)
D2|H2	−0.0122(17)	0.3327(24)	0	0.0575(6)	0.85|0.15
D3|H3	0.0744(11)	0.5104(21)	−0.8752(11)	0.0942(5)	0.48|0.02
D4|H4	0.3717(19)	0.2238(14)	0	0.0288(8)	0.85|0.15
O1	0.2384(8)	0.1498(9)	0.1575(9)	0.0269(4)	1
O2	0.1129(8)	0.0129(9)	0.3266(9)	0.0162(4)	1
O3	0.2630(7)	−0.1101(9)	0.1784(8)	0.0305(4)	1
O4	0.1379(9)	0.0086(1)	0	0.0012(6)	1
Ow1	0.2602(2)	0.0441(2)	0.5	0.0505(6)	1
Ow2	0.5	0	0.0812(49)	0.061(3)	0.5
S|1	0.2385(19)	0.2615(19)	0.25	0.0429(7)	1
T|1	0.1548(17)	0.022(18)	0.1514(15)	0.0339(8)	1

Table 3. Atomic Coordinates, Isotropic Displacement, and Fractional Occupancy Parameters for (Cs, D)−CST

name	z	y	z	U_{iso} (Å^2)	fractional occupancy
Cs1	0.5	0.5	0.25	0.09	0.25
Cs2	0.5	0.5	0.194(1)	0.09	0.25
D1|H1	0.8088(1)	0.3389(2)	0	0.0724(5)	0.76|0.14
D2	0.4228(5)	0.5772(5)	0.1271(7)	0.0724(5)	0.1
D3|H3	0.2035(1)	0.2035(1)	0.3444(1)	0.0407(4)	0.5375|0.275
O1	0.1342(6)	0.3843(5)	0.1698(6)	0.0122(6)	1
O2	0.1161(4)	0.1161(4)	0.3241(5)	0.0142(3)	1
O4	0.1316(8)	0.1316(8)	0	0.0135(3)	1
Ow1	0.3195(1)	0.3195(1)	0.5	0.0615(4)	0.9
Ow2	0.5	0.5	0.5779(4)	0.0615(4)	0.1
Si1	0	0.5	0.25	0.05(1)	1
Ti1	0.1498(1)	0.1498(1)	0.1458(1)	0.065(2)	1

time-resolved in situ data collected subsequently. An unanticipated result of this study was the refinement of a less distorted and more chemically plausible geometry for the interstitial water sites of D−CST than had been previously reported.[27] As described later, the presence of the unidentifiable impurity phase could not be avoided and could not be modeled. Refinements were performed using the programs GSAS[35] and EXP-GUI.[36] Starting atomic positions for refinements were taken from previous X-ray diffraction

(35) Larson, A. C.; VonDreele, R. B. Los Alamos National Laboratory, 2000.

(36) Toby, B. H. *J. Appl. Crystallogr.* **2001**, *34*, 210−213.

Table 4. Selected Bond Lengths and Angles for D−CST[a]

T|1	O1	1.6919(5)	D1|H1	Ow1	1.908(6)
T|1	O2	2.112(8)	D2|H2	Ow1	0.8771(2)
T|1	O2	2.149(7)	D2|H2	Ow2	2.0924(5)
T|1	O2	2.150(7)	D3|H3	Ow2	0.8771(2)
T|1	O3	1.9180(5)	D3|H3	O3	2.3294(8)
T|1	O4	1.8160(7)	D4|H4	O1	2.5215(5)
S|1	O1	1.6556(4)	D4|H4	O2	3.044(1)
S|1	O3	1.6568(4)	D4|H4	Ow1	0.9471(3)
D1|H1	O2	0.813(8)	D4|H4	Ow2	3.014(4)
D2	Ow1	D4	103.049(4)°		
D3	Ow2	D3	116.039(5)°		
Ti1	O2	D1	119.420(2)°		
Ti1	O2	D1	113.232(1)°		
Ti1	O2	D1	11.197(9)°		
Ti1	O2	Ti1	105.404(1)°		
Ti1	O2	Ti1	107.252(1)°		

[a] All distances in Å.

Table 5. Selected Bond Lengths and Angles for (Cs, D)−CST[a]

Ti1	O4	1.7478(5)	D1|H1	Ow1	1.0205(2)
Ti1	O2	2.1554(6)	D1|H1	O1	3.0033(4)
Ti1	O2	2.1381(4)	D2|H2	Ow2	1.0384(0)
Ti1	O1	1.8689(3)	D2|H2	Ow1	1.899(1)
Si1	O1	1.6882(3)	D2|H2	O1	2.7753(3)
Cs1	O1	3.1627(5)	D2|H2	O1	2.7925(2)
Cs2	O1	3.0290(5)	D3|H3	Ow1	2.2568(2)
Cs2	Ow1	3.0588(4)	D3|H3	O2	1.0003(2)
D1|H1	Ow1	D1/H1	107.176(4)°		
D2|H2	Ow2	D2/H2	111.456(1)°		
Ti1	O2	Ti1	102.372(1)°		
Ti1	O2	Ti1	105.651(1)°		
Ti1	O2	D3/H3	94.018(8)°		
Ti1	O2	D3/H3	123.058(3)°		

[a] All distances in Å.

results[2,22,27,37] for the heavy atoms, and from molecular dynamics simulations (Celestian et al. submitted to Nature Materials) for D^+ positions.

The same Rietveld refinement strategy was used for all diffraction patterns. Unit cell, background, and profile parameters were refined first using the Le Bail full pattern decomposition method in GSAS. These parameters were fixed for subsequent Rietveld refinements of the atomic parameters. For time-of-flight data, the diffractometer constant in GSAS (DIFC) was refined for the lower resolution banks at 35° and 90° and fixed for the high-resolution back scattering bank at 145°. The profile function for data collected at Polaris (TOF peak shape function 3 in GSAS) is a convolution of a pseudo-Voigt function with two back-to-back exponentials. For angle-dispersive neutron diffraction data collected at BT-1, a Gaussian function modified for peak asymmetry was used (GSAS profile function 1).[35] Background profiles for the Polaris and BT-1 data were first fit manually, and then a 22−28 term shifted Chebyschev polynomial was applied to interpolate the background profile between the manually selected points. The background in the Polaris data is high due to scattering from water that was not present in the BT-1 data.

Using experimental parameters from the Le Bail fit as a starting point, Rietveld refinements were performed with the scale factor refined first, followed by individual atomic

(37) Poojary, D. M.; Bortun, A. I.; Bortun, L. N.; Clearfield, A. *Inorg. Chem.* **1996**, *35*, 6131−6139.

position, site occupancy, and isotropic displacement parameters. Difference Fourier synthesis maps were calculated (Figure 6) for all least-squares cycles and were used to determine inconsistencies and missing atom sites in the structure model by evaluating nuclear density profiles at 0.1 fractions of the *a*, *b*, *c* unit cell lengths. Peaks in the difference Fourier maps were treated as potential new atomic sites and were assigned atom types on the basis of calculated bond distances and angles with the neighboring atoms. After the Fourier maps were calculated in GSAS, the maps were converted to MCE[38] format, with the GPL'd FOUE software (available at http://www.ccp14.ac.uk/), and used for atom site picking and 3-D display. Once atom sites were labeled, the positions, occupancies, and isotropic displacement parameters were refined individually. Atomic sites that were positionally disordered and sharing the same fractional *x*, *y*, *z* coordinates were constrained to have the same fractional *x*, *y*, *z* coordinates during the refinement. In the final least-squares cycle, Cs isotropic displacement parameters, fractional atomic coordinates, and atomic fractional occupancies were fixed while the remaining atomic site parameters were refined independently (Tables 1−5). Refinement of anisotropic displacement parameters were attempted for all atom positions but resulted in significantly worse χ^2 values of greater than 15.

The determination of the $D/^1H$ ratio in D−CST is straightforward where the amount of proton exchange into Na−CST is established from previous studies.[27,37] After Cs^+ exchange, only 19% of the D/H sites were replaced within 20 min of the start of ion exchange as determined from XRD analysis.[22] The residual charge balance must be supplied from the remaining protons or deuterons on the framework. After 20 min, no further exchange had occurred for the duration of the experiment and it was concluded that maximum exchange was achieved. Structure refinements from XRD data are very sensitive to the presence of Cs^+ because of its high electron density, and accurate chemical compositions can be calculated from these structure models. Obtaining bulk chemical analysis would not be as reliable due to the presence of the impurity phase, and the analysis may underestimate the total amount of Cs^+ present. Structure refinements from neutron diffraction data are not as sensitive to the presence of Cs^+, due to its small neutron scattering length (4.9 fm),[32] so occupancies from XRD analysis are more reliable.

High scattering backgrounds and low total D occupancy from refinements for sites D1 and D3 provided evidence of the presence of ^1H in the samples. Refinement of the $D/^1H$ ratio started with only one isotope, D at site D3, and positions and occupancies were first determined for that site. The refined fractional occupancy for D3 was 0.41(1), while ∼0.81 was expected to satisfy charge balance. The total site occupancy was constrained to total 0.81, while the $D/^1H$ ratio was refined manually. The resulting occupancies were 0.54 and 0.27, respectively, for D and ^1H. The isotope mixing on the water molecule site, Ow1, was refined with the total occupancy constrained at unity. The ratio initially used the

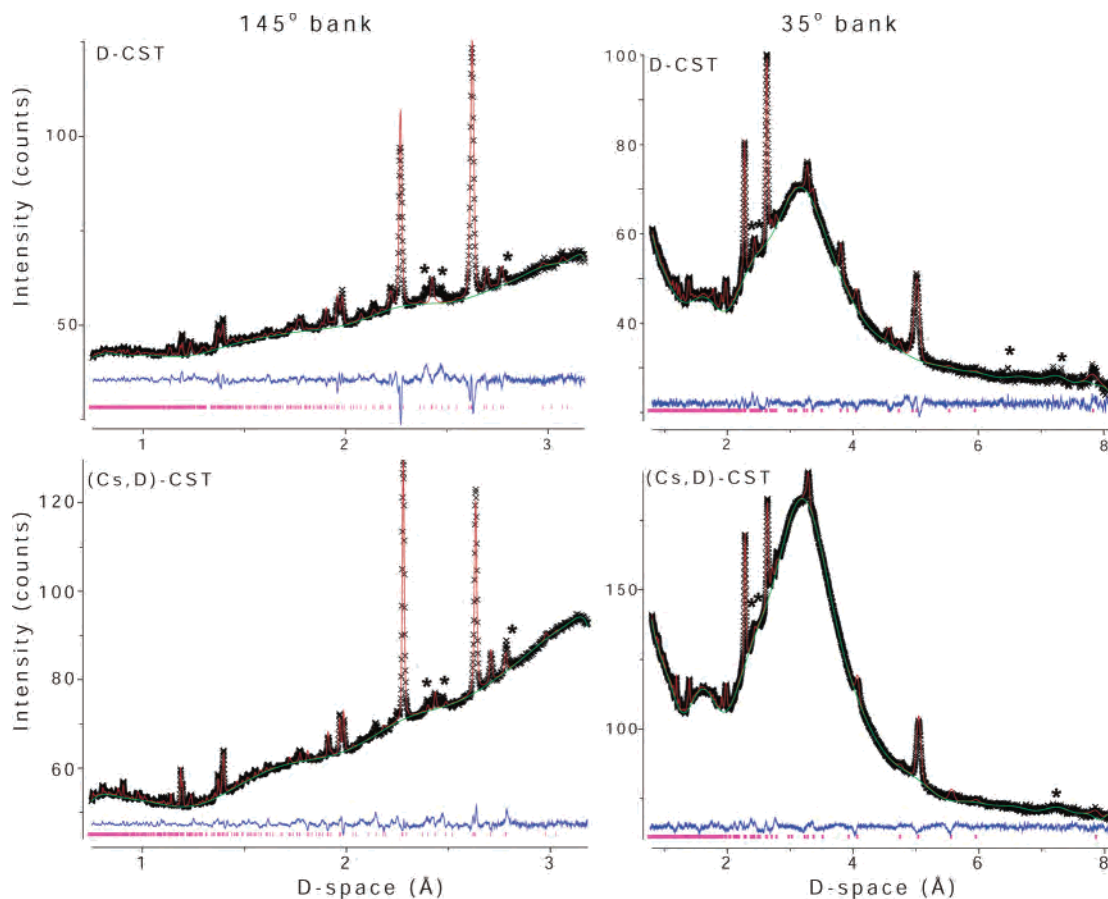(38) Husak, M.; Kratochvil, B. *J. Appl. Crystallogr.* **2003**, *36*, 1104.

Figure 4. Data from time-of-flight diffraction data from the 145° and 35° detector bank of the Polaris beamline at ISIS; the 35° detector bank most clearly illustrates the differences in the D−CST and (Cs, D)−CST diffraction patterns. All data were normalized to the incident beam spectrum. The large background observed in the low-angle detector bank is scattering from liquid D_2O. Scan times were 22 h. for D−CST and 32 h for (Cs, D)−CST. The top figures are for the D−CST structure, and the bottom figures are for the (Cs, D)−CST structure. The unknown impurity phase was not removed, and its reflections are indicated with an asterisk. Collected data (black), calculated profile (red), background (green), difference curve (blue), reflection marks (pink).

D/^{1}H value from the D3|H3 site, but the occupancy for this site, labeled D3 and H3, then refined to 0.76 and 0.14, respectively.

The crystal structure models for D−CST (Figure 1) and (Cs, D)−CST (Figure 7), refined from both time-of-flight and angle-dispersive neutron powder diffraction data (Tables 2 and 3), are in good agreement with previously published structures determined from X-ray[37] and neutron diffraction data,[27] respectively. Average fractional atomic coordinate s.u.'s of all framework sites between D−CST (this study) and H−CST[27] are all within 2σ error. The chemical formula calculated from the Rietveld structure refinements for D−CST and (Cs, D)−CST structures were $D_{1.6}H_{0.4}SiTi_2O_7$·$D_{2.66}H_{0.34}O_{1.5}$ and $Cs_{0.38}D_{1.08}H_{0.54}SiTi_2O_7$·$(D_{1.72}H_{0.28})O$, respectively. Note the prior use of constraints on the chemical formula for charge balance. No evidence was found for the presence of hydronium ions, as suggested by Peterri et al. (1999).[27]

The ion exchange of Cs$^+$ for D$^+$ in the D−CST structure was accompanied by a change in symmetry from space group $P4_2/mbc$ to $P4_2/mcm$ after ~15% site occupancy exchange at Cs2. Description of the structure in space group $P4_2/mcm$ requires a 45° rotation of the unit cell about [001] and reduction in a cell length by ~($\sqrt{2}$)/2 with respect to the unit cell setting in $P4_2/mbc$. The transformation matrix to

transform the unit cell from $P4_2/mbc$ to $P4_2/mcm$ is: **P** = [(0.5, 0.5, 0)(−0.5, 0.5,)(0, 0, 1)].

The more detailed structure for D−CST obtained here confirmed the distorted octahedra and cubane-like units and provides an optimized geometry for the bound water species. The Ti octahedra groups do not form perfect octahedral geometry in the D−CST structure; instead, the Ti^{4+} sites are offset from the octahedron centroid forming longer Ti−O2 bonds (2.13 and 2.18 Å) and shorter Ti−O1 and Ti−O3 (1.69 and 1.91 Å) bonds in the square plane of the octahedron (Table 4). All Ti−O octahedra are edge shared, with Ti−O octahedra groups and having two corners shared with Si tetrahedral groups. The O2 site has four bonds, three with Ti1 and one with D1|H1 forming the deuteroxyl/hydroxyl unit. The Ti_4O_4 cubane-like unit did not form a perfect cube, remaining distorted (Figures 2). The face of the cubane-like unit perpendicular is to [110], [1−10], and [001] has internal Ti−O−Ti angles of 103.35(1)°, 105.26(1)°, and 106.81(1)°. The D−O−O−D dihedral along C in Figure 2 was 4.089-(4)° and along D was 0.605(4)°.

After Cs$^+$ exchange, the positions of the Ti1, Si1, and O1−O4 framework sites of (Cs, D)−CST refined to similar positions to those found in the Cs$^+$ exchanged form of Na−CST,[2] as expected from the L/S ratio of unity for both. The Ti−O octahedra in the (Cs, D)−CST structure are slightly
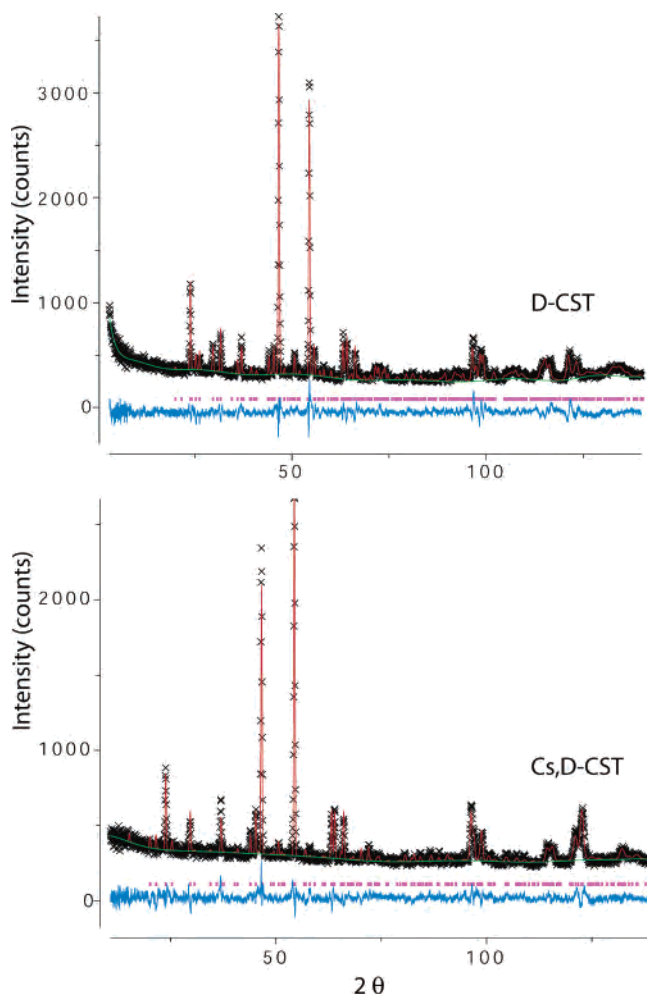
Figure 5. Angle-dispersive neutron diffraction data collected at beamline BT-1 at NCNR NIST. Scan times were 12 h for D−CST and 8 h for (Cs, D)−CST. The top figure is for the D−CST structure, and bottom figure is for the (Cs, D)−CST structure. Unknown impurity phase was not removed. Collected data (black), calculated profile (red), background (green), difference curve (blue), reflection marks (pink).

distorted with long Ti−O [2.1382(3) and 2.1555(5) Å] bonds and short Ti−O [2.7418(2) and 1.869(2) Å] bonds (Table 5). The face of the cubane-like unit perpendicular to [001] in (Cs, D)−CST has internal Ti−O−Ti angles of 102.372-(1)° and the faces parallel to [001] are 105.651(1)°, and exhibits a cubane-like unit less distorted than those of D−CST. The Si−O tetrahedra remained rigid in geometry. Bond valence sum analysis gave increased confidence in the refined (Cs, D)−CST structure (see Appendix for bond valence sum calculations).

Compared to D−CST, the water molecule Ow1 in (Cs, D)−CST moved 0.426(1) Å closer to the center of 8MR (site $x = 0.5$ $y = 0$, $z = 0.25$ in $P4_2/mbc$ setting) and reduced to fractional occupancy of 0.9. Site Ow1 must move closer to the center of 8MR to alleviate the encroached D1−D3 distance which moved from 2.42 Å in D−CST to 2.13 Å in (Cs, D)−CST. The distortion of the D−O bond distances in Ow1 of D−CST now have a more typical and symmetric distance and geometry in (Cs, D)−CST structure of 1.021-(3) Å and D−O−D angle of 107.178(3)°. In addition, the previously unreported water at site Ow2 with fractional occupancy of 0.1, is disordered with site Cs2. From the XRD
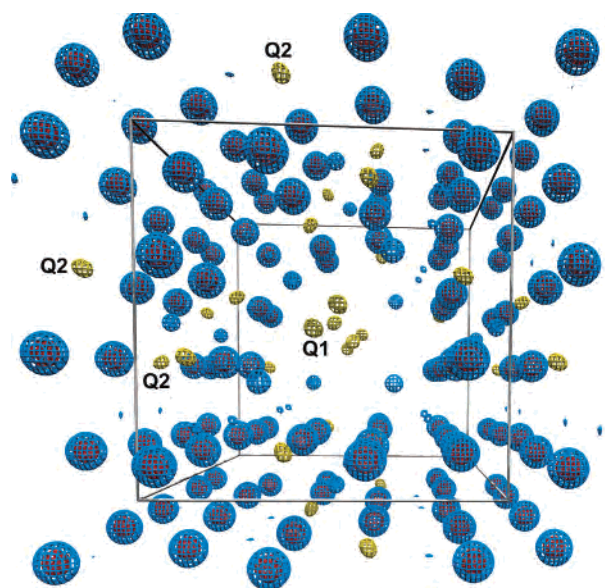

Figure 6. Example of the 3-D calculated Fourier map (red and blue) with difference Fourier map (yellow, peaks Q1 and Q2) used to determine D|H positions in the (Cs, D)−CST phase. Cs⁺ is not shown to clarify Q-peak positions. Density level values are contoured at 2.87 (red), 1.22 (blue), and 0.20 fm/Å³ (yellow), and the unit cell is outlined in gray. The perspective view is parallel to [001]. The peaks Q1 (0.5347 0.5425 0.5) and Q2 (0.1374 0.385575 0.5) do not have any chemically reasonable bond lengths or angles.
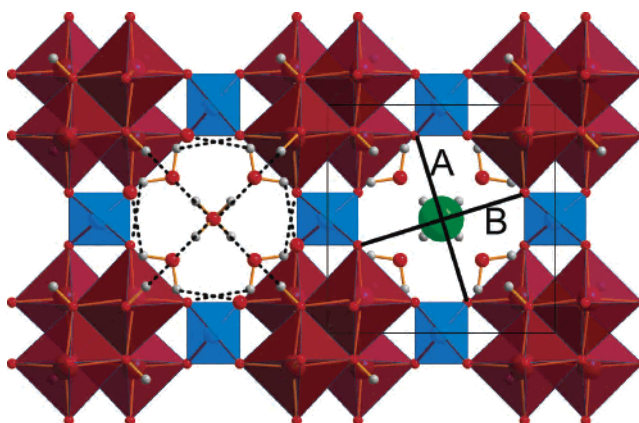

Figure 7. Crystal structure of (Cs, D)−CST from the current study. The view is down the 8MR. The [001] black box is the unit cell. Heavy dashed lines in the left 8MR channel are deuteron bonds from deuteroxyl and water (Ow1), and light dashed lines are deuteron bonds from Ow2 to framework O²⁻. Water deuterons of Ow1 point away the center of the 8MR. Lines B and A are the measured L/S ratio (1.00). Ti (maroon), Si (blue), O (red), H|D (gray).

studies, this water site could not be resolved since the X-ray scattering from Cs⁺ would dominate at this site and low-electron-density species such as O²⁻ and H⁺ would be masked.

The D⁺ sites on the framework have now been determined for (Cs, D)−CST, and these sites are significantly different than those of the D−CST structure. The dihedral of the deuteroxyl groups have moved from ∼4.08° (Figure 2) to a dihedral of ∼47.6° (Figure 8) (vector directions in the $P4_2/mcm$ setting [101], [10−1] [−101], and [−10−1]). The second dihedral when viewed parallel to [010] in D−CST changes from ∼4.66° to 0° in (Cs, D)−CST (viewed parallel to [110] in the $P4_2/mcm$ setting) due to the presence of the

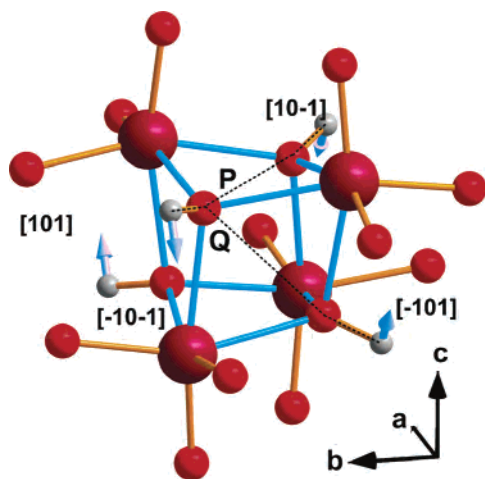**Figure 8.** Cubane-like group of (Cs, D)−CST. Any dihedral angle of D−O−O−D along line Q have an angle of 47.580(2)° and along P are 0°. Solid block arrows indicate the direction D|H moved. The distorted square plane of Ti−O formed from internal Ti−O−Ti face angles perpendicular to [100], [010], and [001] is 105.65(1)°, 105.65(1)°, and 102.37(1)°, respectively. Ti (maroon), O (red), cubane-like unit (blue bonds).

mirror plane and is a consequence of the decreased distortion of the cubane-like unit.

Discussion

The previous time-resolved XRD work had shown that Cs^+ exchange is accompanied by structural transformation, specifically as Cs^+ enters into site Cs2, which forces open the 8MR to make site Cs1 accessible and favored for ion exchange.[22] The mechanism of this transformation was previously unknown because the ${}^1H^+$ positions and the orientations of water and hydroxyl units could not be determined from X-ray diffraction. The opening of the 8MR is illustrated in Figure 1 and shows the polyhedra-column rotations involved in the structural transitions. The Ti−O octahedra columns rotate ∼5.8° as a unit to make the elliptical 8MR (L/S = 1.53) in D−CST to become circular (L/S = 1.0) in (Cs, D)−CST. Corner-shared Si−O tetrahedra and Ti−O octahedra are the more flexible metal−oxygen−metal nodes, and therefore, the bending between the rigid units occurs at their union. The ellipticity of the 6MR's remained unchanged (L/S = 1.25), thus ruling out possible column rotational axes perpendicular to [001]. Rotations of the Ti−O octahedra columns are the most obvious transformation during the Cs^+ exchange process, but it is the origin of the stereochemical changes responsible for the rotations in the columns that are fundamental to the mechanism of the transformation.

The complete structure model obtained here from neutron scattering provides a plausible mechanism underlying the stereochemical changes observed in earlier X-ray studies.[22] Comparison of the D^+ positions in (Cs, D)−CST with those from the D−CST structure refinements reveal that the structural transformation also results in an increased D3−O2−O2−D3 dihedral (line Q in Figure 8) from ∼4.08° to ∼47.6°. The increased dihedral is accompanied by twisting of Ti−O octahedra along the {101} directions. The bending of the deuteroxyl groups are in the direction of column
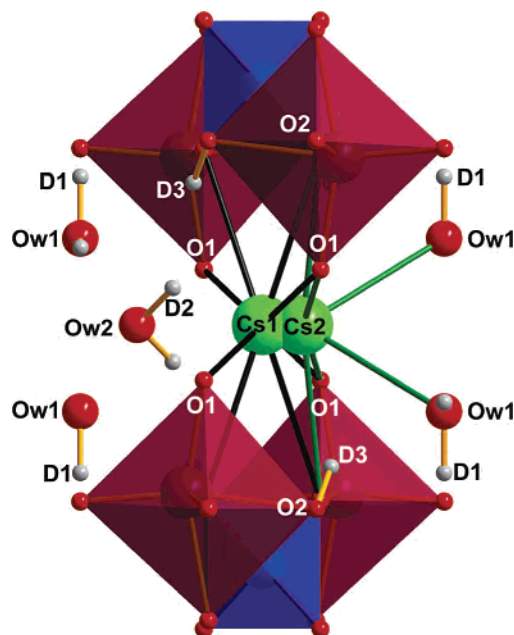
Figure 9. Cross-section view of (Cs, D)−CST 8MR with channel direction in the plane from left to right. 6-fold Cs2-O bonds are shown in green, and 8-fold Cs1−O bonds are shown in black. Silica tetrahedra in-plane with Cs sites, and one Cs2 overlapped with Ow2, were removed for clarity. Sites D3 and D1 are positionally disordered with H3 and H1.

rotation. Since the Ti−O octahedra columns rotate only ∼5.8°, only small distortions of the octahedra are required to change the overall symmetry. This deuteroxyl bending and relaxation of the cubane-like unit is a result of the approach of the water molecule Ow1−D1.

The D1 positions around Ow1 have changed orientation to flip, or rotate, to face the 6MR which is required for the stable hydration of Cs^+ at site Cs2. In the D−CST structure, the D sites on the water point toward the center of the 8MR (Figure 1). This geometry is not possible once Cs^+ enters the lattice, and the water must change orientation to accommodate the Cs2−Ow1 hydration. Once the Ow1 site changes orientation, the D1 sites move furthest away from the Cs sites. Site D1 is forced closer to the intersection of the 8MR and 6MR, and consequently closer to the framework deuteroxyl group, D3. This D1−D3 repulsion is forced and caused the framework deuteroxyl to bend away from the D1 sites on the water.

A second water site (Ow2) was found that has not been previously described for the Cs^+-exchanged phase. Site Ow2 is positionally disordered with Cs2 (Figure 9) with a fractional occupancy of 0.1. The fractional occupancy of this site and that of Ow1 total to one water molecule per formula unit and agree with thermal gravimetric analysis and the X-ray structure model. No water flipping occurs at this site, but the water does rotate ∼25.5° along the [001] direction to maintain the internal D-bonded network due to the change in channel geometry. The plane angle formed between the different orientations of the Ow2 sites changed from 74.44-(1)° to 90°. The water plane angle is the angle between a plane generated by one D2−Ow2−D2 and another plane generated by D2′−Ow2′−D2′ in the same channel but opposing sides of the 8MR (Figures 1 and 7).

Conclusion

From this powder neutron diffraction study, Cs^+ exchange into the 8MR has been found to have two main effects on the D-bond network: (1) The orientation the water molecules are required to flip, or rotate, so that D1 points toward the intersection of the 8MR and 6MR to maximize the distance away from the Cs2 site. This is required to provide the most stable bonding environment for the hydration of Cs2. (2) The D3−O2−O2−D3 dihedral angle increased from 4.089-(2)° to 47.58(2)°. The increase of this dihedral is forced by D1−D3 repulsion by the approaching D on the water molecule Ow1 and forces the Ti−O cubane-like unit to adopt a slightly more cube-like geometry. This relaxation rotates the Ti−O octahedra columns ∼5.8° to form circular 8MR and results in a symmetry change from $P4_2/mbc$ to $P4_2/mcm$. The discovery of a second water molecule in the center of the 8MR may explain the slow filling of the Cs2 site observed during ion exchange as positional disorder with Ow2 is in direct occupancy competition with Cs2. The timing of these events are not well constrained and are being pursued by time-resolved neutron diffraction and molecular dynamics calculations.

Supporting Information Available: Crystallographic information files for D−CST and (Cs, D)−CST and bond valance sum calculations for the (Cs, D)−CST structure. This material is available free of charge via the Internet at http://pubs.acs.org.

IC0611387